Extreme Mechanics Letters 56 (2022) 101875

Contents lists available at ScienceDirect

Extreme Mechanics Letters

journal homepage: www.elsevier.com/locate/eml

Stacking fault induced hardening and grain size effect in nanocrystalline CoNiCrFeMn high-entropy alloy

Renguang Liu [a,b], Jing Tang [a], Jiaxi Jiang [c], Xiaoyan Li [c], Yujie Wei [a,b,*]

[a] LNM, Institute of Mechanics, Chinese Academy of Sciences, Beijing 100190, People's Republic of China
[b] School of Engineering Sciences, University of Chinese Academy of Sciences, Beijing 100049, People's Republic of China
[c] Center for Advanced Mechanics and Materials, Applied Mechanics Laboratory, Department of Engineering Mechanics, Tsinghua University, Beijing 100084, People's Republic of China

ARTICLE INFO

Article history:
Received 5 May 2022
Received in revised form 17 July 2022
Accepted 5 August 2022
Available online 17 August 2022

Keywords:
High entropy alloys
Stacking fault energy
Strengthening
Dislocations
Hall–Petch

ABSTRACT

A broad variation of stacking fault energy (SFE) in high entropy alloys (HEAs) gives rise to rich deformation mechanisms and unique mechanical properties of HEAs. In this paper, we aim to reveal the interplay between grain boundaries and stacking faults in governing the strength and flow stress of CoNiCrFeMn HEA. We carried out atomistic simulations for the tension of polycrystalline CoNiCrFeMn HEA of different grain sizes from 3.0 to 48.6 nm at different temperatures. The tensile flow stress of the HEA follows the traditional Hall–Petch (HP) relation till grain size is down to 15.0 nm. Massive stacking faults contribute to the extra hardening and render a rather gradual drop of flow stress with increasing grain size: In the regime governed by HP relation, partial dislocations emitting from grain boundaries are primarily leading partials; and resulted stacking fault (SF) can serve as barriers to dislocation gliding on intersecting planes. This mild hardening mechanism complements strong hardening from grain boundaries. We expect SF induced hardening could be general in polycrystalline HEAs. The findings reported here may provide a basis and engineering guidance for strengthening and toughening the design of a broad range of HEAs characterized by a wide spectrum of SFEs.

1. Introduction

Guided by the Hall–Petch relation [1,2], grain refinement as an effective strengthening strategy for metals or alloys has been broadly employed. It is therefore natural to question whether novel polycrystalline alloys like high-entropy alloys (HEAs) [3–7] may obey the same relation. Over the past decades, HEAs have been attracting much attention for their outstanding combination of mechanical strength and ductility.

Driven by the ever-increasing demand for high strength and superb deformability, grain size strengthening in face-centered cubic (FCC) CoNiCrFeMn HEAs has been performed experimentally on the micron scale [8,9], even on nanocrystalline regime [10]. In traditional polycrystalline metals, such as Cu [11–13], Fe [14], Ta [15,16] Mg [17], Zr [18], Al [19], it is found that with decreased grain size, the strength of the metals increases to a plateau at an average grain of about ten nanometers followed by a strength softening, a phenomenon termed as inverse Hall–Petch [20,21]. In HEAs, the transition of strength hardening to softening with grain refinement is also broadly observed in $CoNiFeAl_xCu_{1-x}$ [22] and FeNiCrCoCu [23] under tension or compression.

Due to the low SFE in CoNiCrFeMn HEA [24,25], it is easy to nucleate leading partial dislocation bounding a considerable quantity of SFs inside grains. And SFs appear to possibly offer a hardening effect [26]. But how SFs contribute to the unique mechanical properties of HEA, and their interplay with grain-size effect in the nanoscale is still lacking. Due to the difficulty of obtaining detailed deformation behavior in nanocrystalline systems, molecular dynamics (MD) simulation has been adopted broadly, as a complementary tool to experimental investigations. This investigation aims to demonstrate the interaction between dislocations and GBs in HEAs in relatively large grains up to 50 nm and their correlation with strengthening in the presence of low and fluctuating SFEs through MD simulations.

2. Computational methodology

Molecular dynamics simulations with the second nearest-neighbor modified embedded-atom method interatomic potential [27] are performed by using LAMMPS [28]. Initially, twelve cubic simulated samples composed of grains of average grain size d ranging from 3.0, 6.0, 8.0, 10.0, 12.0, 15.0, 20.0, 25.0, 30.0, 38.6, 43.0, and 48.6 nm were prepared. Each model with an average

* Corresponding author at: LNM, Institute of Mechanics, Chinese Academy of Sciences, Beijing 100190, People's Republic of China.
E-mail address: yujie_wei@lnm.imech.ac.cn (Y. Wei).

https://doi.org/10.1016/j.eml.2022.101875

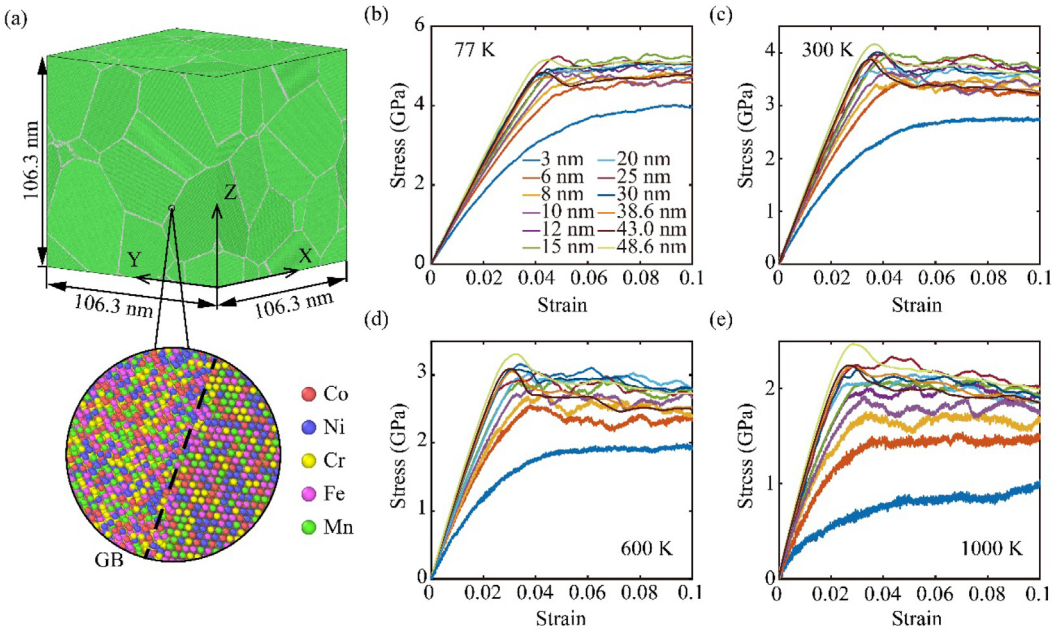

Fig. 1. Stress–strain response of NC CoNiCrFeMn HEA at different temperatures. (a) Typical NC CoNiCrFeMn HEA sample with a close-up view of atomic distribution on GBs, where green atoms have FCC order and white ones are on GBs; in the enlarged region, Co, Ni, Cr, Fe, and Mn atoms are painted in red, blue, yellow, pink, green, respectively; (b) to (e) Stress–strain curves of the NC samples of different grain size at 77, 300, 600, and 1000 K, respectively.

grain size greater than 6.0 nm contains 20 grains, giving rise to a sample size of 16.5 nm ($d = 8.0$ nm) to 106.3 nm ($d = 48.6$ nm), while models with $d = 3.0$ nm and 6.0 nm contain 320 and 40 grains, respectively, to ensure a sample size of 16.5 nm. And all the grains were constructed by the Voronoi construction method to produce random crystallography orientation [29]. Periodic boundary conditions were applied in all directions. And each element shares an equal atomic ratio. A typical microstructure is presented in Fig. 1a, where atoms of different types are colored distinctly with a close-up view of GBs.

The as-prepared samples were relaxed through the energy minimization process using the conjugate gradient method to obtain equilibrium configurations and then heated to specific temperatures of 77, 300, 600, and 1000 K under the NPT ensemble to verify the temperature influence. A uniaxial tension strain of 10% is applied to each sample along the Z-axis over 500 picoseconds, corresponding to a nominal strain rate $\dot{\epsilon} = 2\times10^8$ s^{-1} with constant temperature and zero pressure (stress) along the X- and Y-axis maintained via the NPT ensemble.

3. Results and discussion

3.1. Yield strength and flow stress

Stress–strain curves of samples with various mean grain sizes of CoNiCrFeMn HEA ranging from 3.0 nm to 48.6 nm are shown in Fig. 1b to e for deformation at 77, 300, 600, and 1000 K, in turn. The stress–strain curve of a typical sample resembles what we see in polycrystalline metals: a linear elastic regime at small strains, followed by a nonlinear elastic portion in the stress–strain curve, then a stress plateau; proceeding deformation leads to post-softening (except in the sample of grain size 3.0 nm) and subsequent steady-state plastic flow. Nonlinearity arises from the complex interactions among irregular atomic structures on the boundaries. Massive dislocation nucleation ceases the decrease of stress at a certain strain level and leads to the post-softening. Exception in the sample of small grains (less than 3.0 nm) may attribute to the unperceivable transition between dislocations and GB activities.

The yield stress and flow stress at different temperatures are plotted in Fig. 2 as a function of grain size, the previous results for the common metals are shown in the right column for comparison. The yield stress is obtained by 0.2% offset method, and the flow stress is calculated by averaging the stress at the strain of 6% to 10% where error bars indicate the fluctuations in this strain interval. As shown in Fig. 2, with the temperature rising from 77 K to 1000 K, both stresses decrease significantly.

The left side of Fig. 2a shows the 0.2% yield strength following the conventional definition as a function of grain size. By comparison, we show on the right-hand side the yield strength vs grain size results from other MD simulations. Compared with experimental observations, the HEA deforming at lower temperatures exhibits higher yield strength, originates partly from thermally activated dislocation activities and partly from atomic events at GBs by either diffusive or gliding activities. More strikingly, there is no apparent softening in yield strength as grain size increases at all four temperatures from 77 K to 1000 K, instead, exhibiting the so-called inverse Hall–Petch behavior. At all temperatures, the increase of flow strength is more profound at the smaller size end in contrast to that of large grains, indicating a rapid transition from GB activities in samples of small grains to dislocation-dominated plasticity in samples of larger grains.

The trend in Fig. 2a comes from the competition between GB deformation and dislocation nucleation. At the outset, samples after relaxation are nearly dislocation free. Greater GB volume fraction in samples of smaller grains leads to premature inelastic deformation before 0.2% residual strain for an easier motion of GBs and a greater possibility of partial dislocation emission [30,31], which effectively leads to lower yield strength by the traditional definition. By contrast, large grains are primarily governed by elastic deformation through lattice stretch, in companion with a small amount of inelastic deformation on GBs, and give rise to rather higher yield strength in samples of larger grains. GB mechanisms may become negligible for sufficiently large grains and lead to a saturation of yield strength, as seen in Fig. 2a. Our observations are similar to those reported in the literature [11–19,22,23].

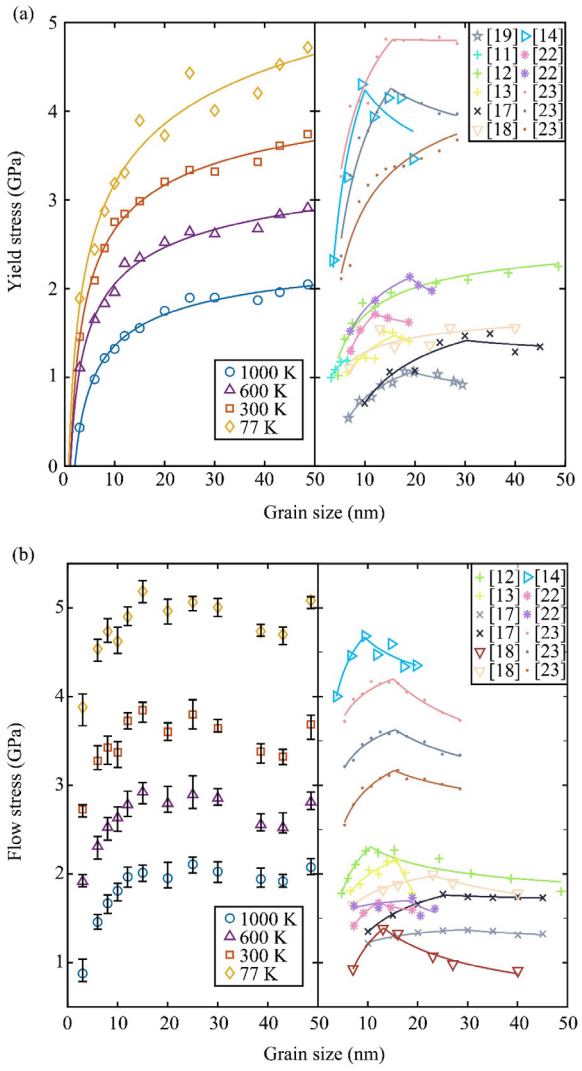

Fig. 2. Stress vs grain size for CoNiCrFeMn HEA at 77, 300, 600, and 1000 K, respectively. (a) Yield stress and (b) flow stress are plotted as a function of the mean grain size of CoNiCrFeMn HEA. Previous results from MD simulations for Cu [11–13], Al [19], Fe [14], Mg [17] (10 K and 300 K), Zr [18] (10 K and 300 K), $CoNiFeAl_xCu_{1-x}$ [22] (FCC and BCC) and CuFeNiCrCo [23] (10 K, 300 K, and 600 K) are shown on the right for comparison.

The flow stress follows the traditional HP relation till grain size down to 15 nm to reach a maximal strength, which are 5.2, 3.8, 2.9, and 2.0 GPa under 77, 300, 600, and 1000 K respectively, as shown in Fig. 2b. Then the flow stress decreases sharply as the grain size is further reduced, on par with previous studies on NC metals [11–19] and HEAs [22,23]. It is worth noting that, the flow stress of CoNiCrFeMn HEAs decreases with increasing grain size, this HP slope is rather mild.

3.2. Evolution of the microstructure

To reveal the mechanism governing the slight size-dependent flow stress, we explore the deformation details and monitor in Fig. 3a to d dislocation activities in one of the grains in the polycrystalline sample with average grain size over 30.0 nm. As seen in Fig. 3a, multiple dislocations with Burgers vector of 1/6<112> nucleate from GB at the applied strain of 4% and then glide across the entire grain till being absorbed by rather than piling up before GB. At this stage, no dislocation interactions are observed, as shown in Fig. 3b. It is of interest to see a prominent feature in this process: the propagating front of the dislocation is highly wavy. Such an irregularity, resulting from nanoscale heterogeneity in terms of atomic composition and resulted energy landscape, plays an important role in the unique mechanical behaviors of HEA and was also observed in previous studies [32]. Please refer to the Appendix Movie (AM 1) to see dislocation nucleation within a grain.

Further deformation leads to a high density of dislocations stored in the grain, as shown in Figs. 3c to d. Interactions between parallel and inclined dislocation give rise to sessile dislocations with Burgers vector of 1/6<110> (Fig. 3d, lines in purple). It is noted that the 1/6<112> dislocation is the most common partial in FCC metals, bounding a stacking fault which may influence both dislocation nucleation and motion, in addition to preexisting GBs.

3.3. Stacking fault induced hardening

The blocking effect on dislocations imposed by stacking faults is further demonstrated in Figs. 3e to h. In the early stage of plastic deformation, leading partials are nearly on parallel slip planes, as found in Figs. 3e and f. Very few trailing partials are seen to follow those leading partials emitted from GBs. Later on, deformation activates dislocation activities in all three distinct slip planes with distinct normal, shown in Figs. 3g and h (see AM 2 for the nucleation process of the SF network within a grain). Their interaction and intersection give rise to fine plastically deformed domains, akin to those seen in twin-induced plasticity steels (TWIP) under plastic deformation [33] as well as in maraging steels with ultrafine and dense nanoscale precipitates [34,35].

The subsequent partials in intersecting planes either penetrate the previous SFs or being blocked, forming narrowly spaced stacking fault networks. The atomic nature of such a process is demonstrated in Figs. 4a to c. We show in Fig. 4a an incident 1/6<112> leading partial run into a preexisting SF, which in turn serves as a barrier to the leading partial until accumulative energy reaches a new high to let it break-in. The penetrated segment continues to propagate with further straining. Incident leading partials are not necessarily able to penetrate the stacking faults, which may lead to a blocking mechanism (see Fig. 4d and AM 3), evidence of hardening induced by stacking fault. Alternatively, it may form a sessile stair-rod dislocation with another partial (see Fig. 4e) which is thought to stabilize the SF network [36] and also strengthen the material at some level. These two mechanisms originated from stacking faults, in combination supply extra hardening mechanisms in addition to existing unveiled ones.

Since SFs may serve as barriers to dislocation motion, in resemble of planar structures like twin boundaries, we are interested in its density evolution during deformation. In Fig. 5, we present both mean stacking fault spacing (SFS) and dislocation density. The evolution of both with loading is shown in the right column, and their average values at strain of 6% to 10% are plotted in the left column as a function of grain size. The SFS is approximated by counting the number of HCP atoms on stacking faults N_{SF} in a sample. Taking account the number of atoms in one cross-sectional atomic plane is N_s, a total number of stacking fault planes is estimated to be $n = \frac{N_{SF}}{N_s}$, from which we obtain the average SFS l through $(nl)^3 \approx V$ for V being the volume of simulation box.

From Fig. 5a, we see that the SFS decreases rapidly from 50 Å to 15 Å as grain size is up to 20 nm, and the space becomes stable with further grain size increases. It may suggest saturated hardening by stacking faults beyond grains greater than 20 nm. Stacking fault spacing decreases with straining at both 77 K and 600 K, as shown in Figs. 5b and c.

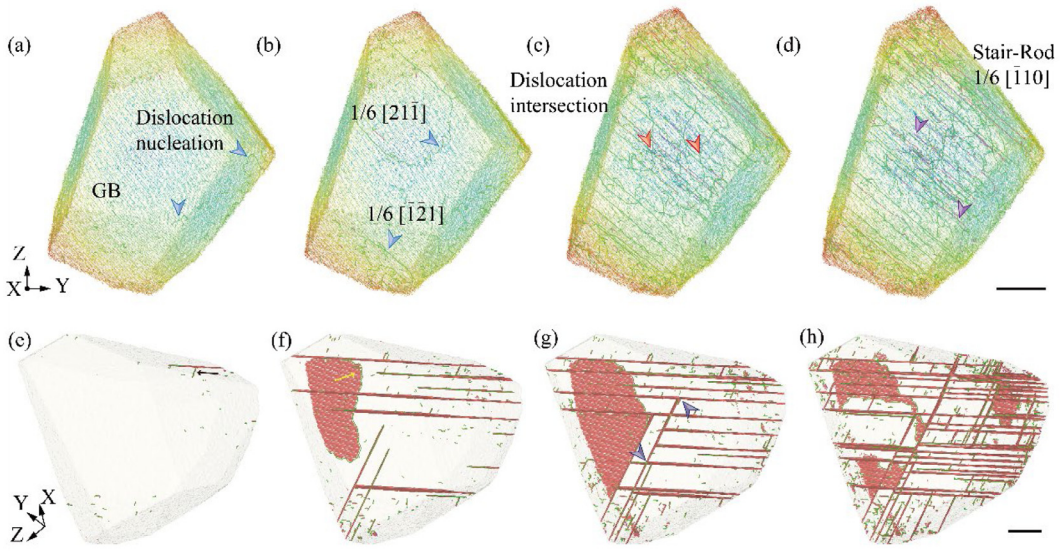

Fig. 3. Snapshots of a grain in the polycrystalline CoNiCrFeMn HEA with $d = 38.6$ nm under 77 K and at the applied strain of (a) 4%, (b) 5%, (c) 8%, and (d) 10%, respectively, where FCC and HCP atoms were invisible. Remaining atoms were colored according to the distance to the center. The solid lines are dislocations identified by the dislocation extraction method, where green (purple) dislocation type was 1/6<112> (1/6<110>). To show the structures of stacking faults, a grain with $d = 48.6$ nm at the applied strain of (e) 4%, (f) 5%, (g) 6%, and (h) 10% is further presented, where only HCP atoms remained. The arrows point to interactions of stacking faults. (Scale bar=10 nm.)

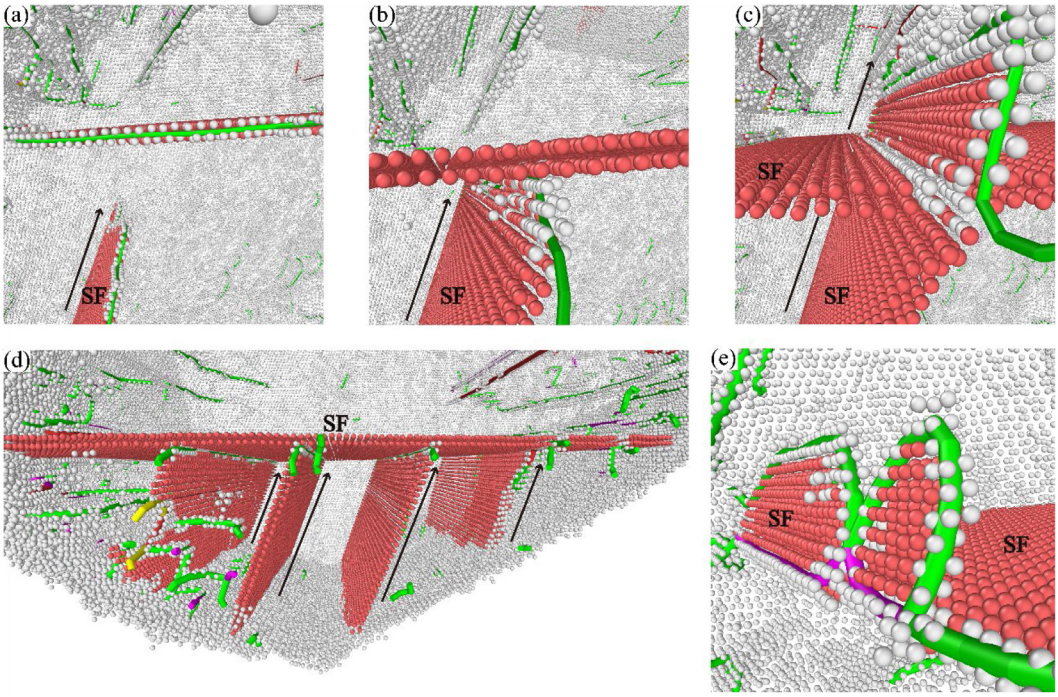

Fig. 4. The interactions between dislocations or SFs on intersecting planes. (a–c) A partial dislocation penetrates through SFs at further strain 7.6%, 7.7%, and 8.1%, respectively. (d) The blocked partials by SF. (e) A stair-rod dislocation with Burgers vector of 1/6<110> formed by two partials. The arrows indicate the slip directions of partials.

The densities of total dislocations ρ are presented in Figs. 5d and e. Higher temperature certainly facilitates the nucleation of dislocations, as evidently seen by comparing Fig. 5e with f. Samples are nearly dislocation free at 77 K before 4% strain but there emerges a large amount of dislocation when samples are deformed at 600 K and at the same strain level. The average dislocation density rises sharply as grain size increases to ~15.0 nm, and it then decreases, in compatible with the trend of flow stress vs grain size seen in Fig. 2b. Please refer to AM 4 and 5 for dislocation activities in samples of grain size about 12.0 nm and 38.6 nm, respectively.

4. Conclusion

Stacking fault energy plays a central role in the mechanical properties of FCC metals, including the brittle-to-ductile

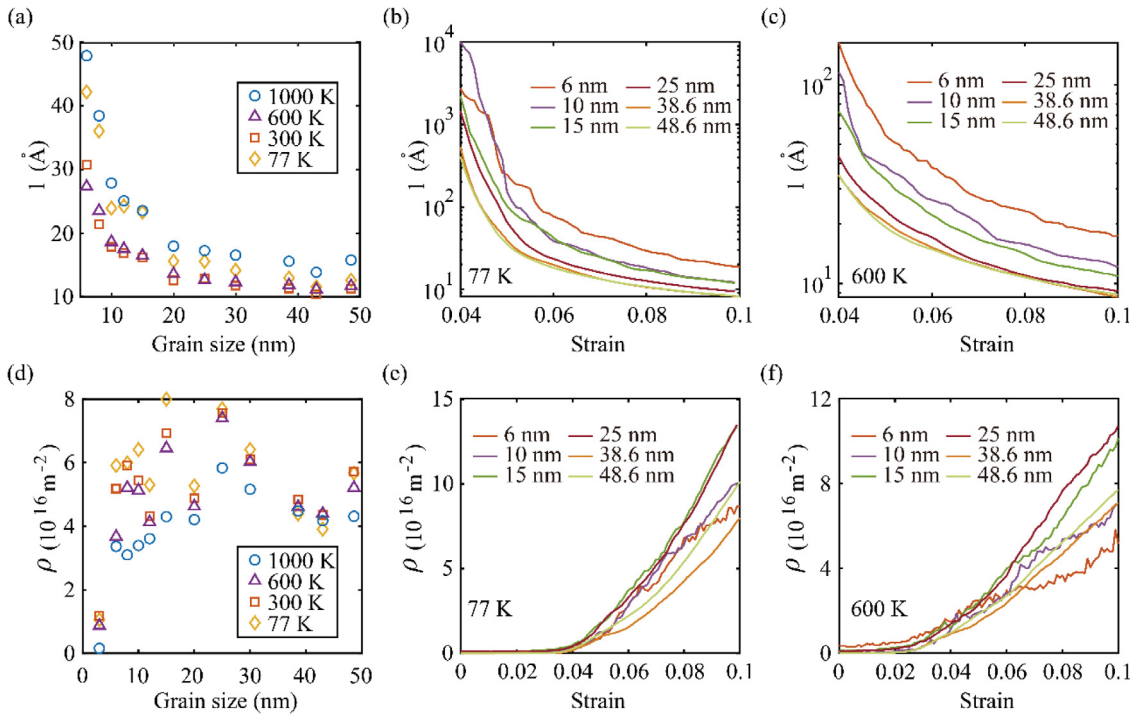

Fig. 5. Statistics of stacking fault spacing (SFS) and dislocation density. (a) SFS versus grain size under uniaxial tension at the strain of 6% to 10%. SFS versus strains for samples of several grain size deforming at (b) 77 K and (c) 600 K. (d) The densities of averaged dislocations ρ at the strain of 6% to 10% as a function of average grain size. (e) ρ versus strain at 77 K, (f) ρ versus strain at 600 K.

transition in materials [37], the partial-to-complete dislocation transition and its implication with fracture toughness [38,39], the dislocation-to-twinning deformation in TWIP steels [33], and the phase transformation in TRIP steels [40]. High entropy alloys supply a material system all those features may co-exist and be tunable to achieve superb properties: as a consensus, SFE in HEA follows a wide span of distribution through chemical and structural manipulation. Such broad distribution of SFE makes HEAs unique in many aspects and has been under intensive exploration since its discovery [41].

In this paper, we revealed the interplay between GBs and stacking faults in governing the strength and flow stress of CoNiCrFeMn HEA. We carried out atomic simulations of polycrystalline CoNiCrFeMn HEA of different grain sizes from 3.0 to 48.6 nm. The tensile flow stress of the HEA follows the traditional Hall–Petch relation till grain size down to 15.0 nm. A mass of stacking faults contributes to the extra hardening and renders a rather gradual drop of flow stress with increasing grain size. In the regime governed by the Hall–Petch relation, partial dislocations emitting from GBs are primarily leading partials. Three distinct slip planes are commonly activated in modeled samples of large grains: partial dislocations in intersecting planes either penetrate the previous SFs or being blocked, forming narrowly spaced SF networks. Resulted SF can serve as barriers to dislocation gliding on intersecting planes. There are a large number of stair-rod dislocations with Burgers vector of 1/6<110> as well, which are considered to stabilize the SF network and strengthen the material at some level. These two mechanisms originated from SFs complements with strong hardening from GBs. To conclude, we expect SF induced hardening could be general in polycrystalline HEAs. The findings reported here may provide a basis and engineering guidance for strengthening and toughening design of a broad range of HEAs characterized by a wide spectrum of distribution of low SFEs.

Declaration of competing interest

The authors declare that they have no known competing financial interests or personal relationships that could have appeared to influence the work reported in this paper.

Data availability

Data will be made available on request.

Acknowledgments

The authors acknowledge support from the National Natural Science Foundation of China (NSFC) Basic Science Center for ‘Multiscale Problems in Nonlinear Mechanics’ (No. 11988102).

Appendix A. Supplementary data

Supplementary material related to this article can be found online at https://doi.org/10.1016/j.eml.2022.101875.

References

[1] E.O. Hall, The deformation and ageing of mild steel: III discussion of results, Proc. Phys. Soc. B 64 (1951) 747–753, http://iopscience.iop.org/0370-1301/64/9/303.
[2] Petch, Nuclear composition-a factor of interest in nucleation, Act. Metall. 1 (1953) 764–766.
[3] J.W. Yeh, S.K. Chen, S.J. Lin, J.Y. Gan, T.S. Chin, T.T. Shun, C.H. Tsau, S.Y. Chang, Nanostructured high-entropy alloys with multiple principal elements: Novel alloy design concepts and outcomes, Adv. Eng. Mater. 6 (2004) 299–303, http://dx.doi.org/10.1002/adem.200300567.
[4] M.H. Tsai, J.W. Yeh, High-entropy alloys: A critical review, Mater. Res. Lett. 2 (2014) 107–123, http://dx.doi.org/10.1080/21663831.2014.912690.
[5] Q. Fang, Y. Chen, J. Li, C. Jiang, B. Liu, Y. Liu, P.K. Liaw, Probing the phase transformation and dislocation evolution in dual-phase high-entropy alloys, Int. J. Plasticity 114 (2019) 161–173, http://dx.doi.org/10.1016/j.ijplas.2018.10.014.

[6] D.B. Miracle, O.N. Senkov, A critical review of high entropy alloys and related concepts, Act. Mater. 122 (2017) 448–511, http://dx.doi.org/10.1016/j.actamat.2016.08.081.
[7] Y.F. Ye, Q. Wang, J. Lu, C.T. Liu, Y. Yang, High-entropy alloy: challenges and prospects, Mater. Today 19 (2016) 349–362, http://dx.doi.org/10.1016/j.mattod.2015.11.026.
[8] J. He, Q. Wang, H. Zhang, L. Dai, T. Mukai, Y. Wu, X. Liu, H. Wang, T.G. Nieh, Z. Lu, Dynamic deformation behavior of a face-centered cubic FeCoNiCrMn high-entropy alloy, Sci. Bull. 63 (2018) 362–368, http://dx.doi.org/10.1016/j.scib.2018.01.022.
[9] S.J. Sun, Y.Z. Tian, H.R. Lin, X.G. Dong, Y.H. Wang, Z.J. Wang, Z.F. Zhang, Temperature dependence of the Hall–Petch relationship in CoCrFeMnNi high-entropy alloy, J. Alloys Compounds 806 (2019) 992–998, http://dx.doi.org/10.1016/j.jallcom.2019.07.357.
[10] H. Gleiter, Nanocrystalline materials, Prog. Mater. Sci. 33 (1989) 223–315.
[11] J. Schioøtz, K.W. Jacobsen, A maximum in the strength of nanocrystalline copper, Science 301 (2003) (1979) 1357–1359, http://dx.doi.org/10.1126/science.1086636.
[12] Jakob Schiøtz, Francesco D. Di Tolla, Karsten W. Jacobsen, Softening of nanocrystalline metals at very small grain sizes, Nature 391 (1998) 561–563.
[13] M. Zhang, Z. Rao, T. Xu, L. Fang, Quantifying the influence of grain boundary activities on Hall-Petch relation in nanocrystalline Cu by using phase field and atomistic simulations, Int. J. Plasticity 135 (2020) http://dx.doi.org/10.1016/j.ijplas.2020.102846.
[14] J.B. Jeon, B.J. Lee, Y.W. Chang, Molecular dynamics simulation study of the effect of grain size on the deformation behavior of nanocrystalline body-centered cubic iron, Scripta Mater. 64 (2011) 494–497, http://dx.doi.org/10.1016/j.scriptamat.2010.11.019.
[15] Y. Tang, E.M. Bringa, M.A. Meyers, Inverse Hall-Petch relationship in nanocrystalline tantalum, Mater. Sci. Eng. A 580 (2013) 414–426, http://dx.doi.org/10.1016/j.msea.2013.05.024.
[16] Z. Pan, Y. Li, Q. Wei, Tensile properties of nanocrystalline tantalum from molecular dynamics simulations, Acta Mater. 56 (2008) 3470–3480, http://dx.doi.org/10.1016/j.actamat.2008.03.025.
[17] H.Y. Song, Y.L. Li, Atomic simulations of effect of grain size on deformation behavior of nano-polycrystal magnesium, J. Appl. Phys. 111 (2012) http://dx.doi.org/10.1063/1.3687908.
[18] C.J. Ruestes, G. Bertolino, M. Ruda, D. Farkas, E.M. Bringa, Grain size effects in the deformation of [0 0 0 1] textured nanocrystalline Zr, Scripta Mater. 71 (2014) 9–12, http://dx.doi.org/10.1016/j.scriptamat.2013.09.010.
[19] W. Xu, L.P. Dávila, Tensile nanomechanics and the Hall-Petch effect in nanocrystalline aluminium, Mater. Sci. Eng. A 710 (2018) 413–418, http://dx.doi.org/10.1016/j.msea.2017.10.021.
[20] M.A. Meyers, A. Mishra, D.J. Benson, Mechanical properties of nanocrystalline materials, Prog. Mater. Sci. 51 (2006) 427–556, http://dx.doi.org/10.1016/j.pmatsci.2005.08.003.
[21] A.H. Chokshi, A. Rosen, J. Karch, H. Gleiter, On the validity of the Hall-Petch relationship in nanocrystalline materials, Scripta Metall. 23 (1989) 1679–1684.
[22] S. Chen, Z.H. Aitken, Z. Wu, Z. Yu, R. Banerjee, Y.W. Zhang, Hall-Petch and inverse Hall-Petch relations in high-entropy CoNiFeAlxCu1-x alloys, Mater. Sci. Eng. A 773 (2020) http://dx.doi.org/10.1016/j.msea.2019.138873.
[23] L. Zhang, Y. Shibuta, Inverse Hall-Petch relationship of high-entropy alloy by atomistic simulation, Mater. Lett. 274 (2020) http://dx.doi.org/10.1016/j.matlet.2020.128024.
[24] S. Huang, W. Li, S. Lu, F. Tian, J. Shen, E. Holmström, L. Vitos, Temperature dependent stacking fault energy of FeCrCoNiMn high entropy alloy, Scripta Mater. 108 (2015) 44–47, http://dx.doi.org/10.1016/j.scriptamat.2015.05.041.
[25] S. Liu, Y. Wei, The Gaussian distribution of lattice size and atomic level heterogeneity in high entropy alloys, Extreme Mech. Lett. 11 (2017) 84–88, http://dx.doi.org/10.1016/j.eml.2016.10.007.
[26] Z. Zhang, Q. Fu, J. Wang, P. Xiao, F. Ke, C. Lu, Hardening Ni3Al via complex stacking faults and twinning boundary, Comput. Mater. Sci. 188 (2021) http://dx.doi.org/10.1016/j.commatsci.2020.110201.
[27] W.M. Choi, Y.H. Jo, S.S. Sohn, S. Lee, B.J. Lee, Understanding the physical metallurgy of the CoCrFeMnNi high-entropy alloy: An atomistic simulation study, Npj Comput. Mater. 4 (2018) http://dx.doi.org/10.1038/s41524-017-0060-9.
[28] S. Plimpton, Computational limits of classical molecular dynamics simulations, 1995.
[29] A.G. Frøseth, H. van Swygenhoven, P.M. Derlet, Developing realistic grain boundary networks for use in molecular dynamics simulations, Acta Mater. 53 (2005) 4847–4856, http://dx.doi.org/10.1016/j.actamat.2005.06.032.
[30] R. Li, H.B. Chew, Grain boundary traction signatures: Quantifying the asymmetrical dislocation emission processes under tension and compression, J. Mech. Phys. Solids 103 (2017) 142–154, http://dx.doi.org/10.1016/j.jmps.2017.03.009.
[31] R. Li, H.B. Chew, Grain boundary traction signatures: Quantitative predictors of dislocation emission, Phys. Rev. Lett. 117 (2016) http://dx.doi.org/10.1103/PhysRevLett.117.085502.
[32] Q.J. Li, H. Sheng, E. Ma, Strengthening in multi-principal element alloys with local-chemical-order roughened dislocation pathways, Nat. Commun. 10 (2019) http://dx.doi.org/10.1038/s41467-019-11464-7.
[33] R.A. Cooper, Y. Wang, B. Vignolle, O.J. Lipscombe, S.M. Hayden, Y. Tanabe, T. Adachi, Y. Koike, M. Nohara, H. Takagi, C. Proust, N.E. Hussey, Anomalous criticality in the electrical resistivity of La 2-xSrxCuO4, Science 323 (2009) (1979) 603–607, http://dx.doi.org/10.1126/science.1165015.
[34] S. Jiang, H. Wang, Y. Wu, X. Liu, H. Chen, M. Yao, B. Gault, D. Ponge, D. Raabe, A. Hirata, M. Chen, Y. Wang, Z. Lu, Ultrastrong steel via minimal lattice misfit and high-density nanoprecipitation, Nature 544 (2017) 460–464, http://dx.doi.org/10.1038/nature22032.
[35] S. Peng, Y. Wei, H. Gao, Nanoscale precipitates as sustainable dislocation sources for enhanced ductility and high strength, PANS (2020) 1–6, http://dx.doi.org/10.1073/pnas.1914615117/-/DCSupplemental.
[36] S. Chen, H.S. Oh, B. Gludovatz, S.J. Kim, E.S. Park, Z. Zhang, R.O. Ritchie, Q. Yu, Real-time observations of TRIP-induced ultrahigh strain hardening in a dual-phase CrMnFeCoNi high-entropy alloy, Nat. Commun. 11 (2020) http://dx.doi.org/10.1038/s41467-020-14641-1.
[37] J.R. Rice, R. Thomson, Ductile versus brittle behaviour of crystalst, Philosophical Mag. 29 (1974) 73.
[38] E.B. Tadmor, S. Hai, A Peierls criterion for the onset of deformation twinning at a crack tip, J. Mech. Phys. Solids 51 (2003) 765–793, http://dx.doi.org/10.1016/S0022-5096(03)00005-X.
[39] James R. Rice, Dislocation nucleation from a crack tip: An analysis based on the Peierls concept, J. Mech. Phys. Solids 40 (1992) 239–271.
[40] Z. Li, K.G. Pradeep, Y. Deng, D. Raabe, C.C. Tasan, Metastable high-entropy dual-phase alloys overcome the strength-ductility trade-off, Nature 534 (2016) 227–230, http://dx.doi.org/10.1038/nature17981.
[41] J.W. Yeh, S.K. Chen, S.J. Lin, J.Y. Gan, T.S. Chin, T.T. Shun, C.H. Tsau, S.Y. Chang, Nanostructured high-entropy alloys with multiple principal elements: Novel alloy design concepts and outcomes, Adv. Eng. Mater. 6 (2004) 299–303, http://dx.doi.org/10.1002/adem.200300567.